

Temperature dependence of the collective mode and its influence on the band splitting in bilayer cuprates

S. Varlamov and G. Seibold

Institut für Physik, BTU Cottbus, PBox 101344, 03013 Cottbus, Germany

(Dated: November 21, 2018)

The recently observed bilayer splitting in high- T_c cuprates is analyzed within a model where the charge carriers are coupled to a phenomenological bosonic spectrum which interpolates between the marginal Fermi liquid structure and collective mode type behavior as a function of temperature. We argue that the origin of the collective mode is associated with dynamic incommensurate charge density waves. Moreover it is shown that the resulting temperature dependence of the self-energy Σ is in good agreement with that extracted from angle-resolved photoemission data.

PACS numbers: 74.25.Jb, 74.72.Hs, 74.20.Mn

I. INTRODUCTION

One of the long standing unsolved problems in angle-resolved photoemission spectroscopy (ARPES) of high- T_c cuprates was the detection of band doubling in bilayer materials. In these compounds one naturally expects a splitting of the quasiparticle (QP) dispersion in an antibonding (AB) and bonding band (BB) due to finite hopping of charge carriers between the two CuO_2 planes. Only recently this feature has been measured in $\text{Bi}_2\text{Sr}_2\text{CaCu}_2\text{O}_{8+\delta}$ ($\text{Bi}2212$)^{1,2,3} above and below T_c . The splitting turns out to be essentially zero along the diagonals $(0,0) \rightarrow (\pi,\pi)$ and (in the normal state) acquires a value between 88meV^1 and 110meV^2 at the $(\pi,0)$ point of the Brillouin zone (BZ). In addition it seems that the magnitude of the energy splitting is constant over a large range of doping.⁴ Most interestingly it turns out that for the same doping the splitting is only 22meV below T_c ¹ contrary to the expectation that the hopping between planes t_\perp should be essentially temperature independent.

In this paper we show that the apparent reduction of the bilayer splitting below T_c can be explained by the assumption that the charge carriers are coupled to bosons which frequency distribution evolves from a featureless structure well above T_c (i.e. approaching that of a marginal Fermi liquid⁵) to a sharp, mode-like excitation at small temperatures. As a consequence, low energy QP excitations are essentially confined to energies up to the mode frequency ω_0 which thus constitutes an upper limit for the splitting between AB and BB QP peaks (see Fig. 4). Moreover, the damping of excitations for energies larger than ω_0 leads to a broad hump which turns out to be mainly determined by the bonding band (cf. Fig. 3c). This scenario is thus in agreement with recent ARPES experiments³ where this peak-dip hump structure at $(\pi,0)$ has been resolved below T_c in addition to the bilayer splitting.

Numerous experiments now support the existence of a collective mode in the high- T_c materials most prominently exemplified by the appearance of a kink in the electron dispersion along $(0,0) \rightarrow (\pi,\pi)$ as seen in ARPES^{6,7} (cf. also Fig. 2). Concerning the origin of the mode the

various proposals include a magnetic resonance (see e.g. Ref. 8), the coupling to phonons⁷ or incommensurate charge-density waves (ICDW)⁹ as the source of the associated scattering. It has been argued⁸ that the difference between peak and dip position of the photoemission line shape at $(\pi,0)$ decreases as a function of doping as it is expected for the magnetic resonance frequency. An analogous analysis⁷ came to the conclusion that the frequency is essentially constant (if not slightly decreasing) upon doping thus resembling the behavior of a phonon mode. We have recently fitted¹¹ ARPES data taking into account also the feedback of the doping dependent superconducting (SC) gap. The extracted mode frequency is a strongly decreasing function of hole concentration reaching a value of $\omega \sim 40\text{meV} \dots 50\text{meV}$ around optimal doping. This behavior is thus consistent with a quantum critical point (QCP) located near optimal doping where the associated order parameter corresponds to ICDW formation.¹⁰ In fact, the formation of stripe order is now well established in a large class of cuprate compounds (for an overview see e.g. Ref. 13). Most interestingly the coexistence of charge modulations and superconductivity has recently also been reported for the $\text{Bi}2212$ compound using scanning tunneling microscopy.^{14,15} These experiments strongly support our view that ICDW scattering can also be responsible for the mode-like features as seen in ARPES experiments. In the following we substantiate this scenario by a detailed analysis of the temperature dependent collective mode which allows us to fit the experimentally observed bilayer splitting in the superconducting and normal state respectively by simply tuning the broadening of our phenomenological bosonic spectrum.

The paper is organized as follows. In Sec. II we analyze available experimental data in order to elucidate the frequency and temperature dependence of the collective mode in $\text{Bi}2212$ materials. Based on these results the temperature dependent bilayer splitting is investigated within the ICDW mode scenario in Sec. III. We finally conclude our discussion in Sec. IV.

II. TEMPERATURE DEPENDENCE OF THE COLLECTIVE MODE

The coupling of charge carriers to a collective mode is reflected in a drop of the imaginary part of the electronic self-energy $\text{Im } \Sigma$ below some characteristic mode frequency ω_0 . In Refs. 16,17 the ARPES line width, which is directly related to $\text{Im } \Sigma$, has been analyzed for an optimally doped Bi2212 sample ($T_c=90\text{K}$) as a function of frequency and temperature. In fact, it was observed that in the SC state $\text{Im } \Sigma$ is strongly reduced below $70\dots 80\text{meV}$ which compares rather well with the drop of the scattering rate as obtained from infrared reflectivity measurements.¹⁸ Moreover, with increasing temperature there is a gradual change of $\text{Im } \Sigma$ towards a linear frequency dependence above T_c . The corresponding marginal Fermi liquid (MFL) structure of the ARPES line shape is also discussed in Ref. 19.

In order to interpolate between these two limiting self-energies we consider the coupling of charge carriers to the following bosonic spectrum:

$$B(\omega) = \tanh(\omega/(kT))F_{\omega_0,\Gamma}(\omega) \quad (1)$$

where $F_{\omega_0,\Gamma}(\omega)$ is a normalized distribution function centered around ω_0 with halfwidth Γ . Assuming particle-hole symmetry with respect to the chemical potential and neglecting for the moment the influence of the SC gap²⁰, evaluation of the $T = 0$ self-energy yields

$$\text{Im}\Sigma(\omega) = \lambda^2 N(0) \int_0^{\min(-\omega,\omega_c)} d\nu F_{\omega_0,\Gamma}(\nu) \quad (2)$$

$$\text{Re}\Sigma(\omega) = -\lambda^2 N(0) \int_0^{\omega_c} d\nu F_{\omega_0,\Gamma}(\nu) \ln \left| \frac{\nu + \omega}{\nu - \omega} \right| \quad (3)$$

Here λ denotes the coupling constant, $N(0)$ corresponds to the density of states at the chemical potential and ω_c is an upper cutoff energy for the interaction.

In the limit $\Gamma \rightarrow 0$ where $F_{\omega_0,\Gamma \rightarrow 0}(\omega) = \delta(\omega - \omega_0)$ Eqs. (2,3) describe the self-energy as arising from the coupling to a single oscillator mode. In this case one obtains the well-known step-function behavior²² of $\text{Im } \Sigma(\omega) = 1/2\lambda^2 N(0)\Theta(|\omega| - \omega_0)$. Let us consider for illustrative purposes at first a rectangular distribution function $F_{\omega_0,\Gamma}(\omega)$ with halfwidth Γ and height $1/(2\Gamma)$ for which the self-energy can be calculated analytically. As a result for finite but small $\Gamma < \omega_0$ the step in $\text{Im } \Sigma(\omega)$ will evolve into a linear increase between $\omega_0 - \Gamma$ and $\omega_0 + \Gamma$. Finally for $\Gamma = \omega_0$ the MFL limit is reached where $\text{Im } \Sigma(\omega) \sim \omega$ for $0 < \omega < \omega_0 + \Gamma$.

Furthermore we evaluate the quasiparticle weight $Z = (1 - (\partial\Sigma/\partial\omega)_{\omega=0})^{-1}$ which is given by

$$Z = \left[1 + \frac{\lambda^2 N(0)}{\Gamma} \ln \frac{\omega_0 + \Gamma}{\omega_0 - \Gamma} \right]^{-1} \quad (4)$$

and vanishes logarithmically when Γ approaches the mean mode frequency ω_0 . This result can be connected

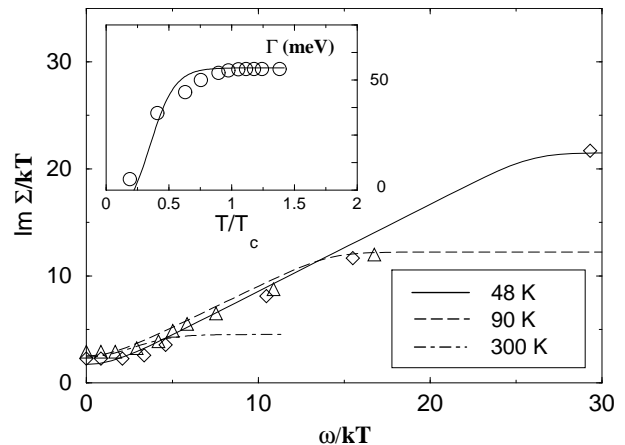


FIG. 1: $\text{Im } \Sigma/kT$ as a function of ω/kT for 48 K (solid line, diamonds), 90 K (dashed line, triangles) and 300 K (dotted-dashed line). Symbols are experimental data taken from Fig. 4 of Ref. 6. Inset: $\Gamma(T)$ as obtained from a comparison between eq. (4) and experimental data of Ref. 12 (circles).

with recent ARPES experiments where the quasiparticle weight Z as a function of temperature has been extracted from the line shape at $(\pi, 0)$.¹² In fact it was found that Z drops significantly as temperature approaches T_c with a small but nonzero Z also above T_c . From Eq. (4) we thus conclude that the bosonic spectrum is governed by a distribution function $F_{\omega_0,\Gamma}(\omega)$ with a strongly temperature dependent halfwidth $\Gamma = \Gamma(T)$.

We have extracted $\Gamma(T)$ by comparing eq. (4) with the experimentally determined quasiparticle weight (Fig. 4b in Ref. 12). The result is displayed in the inset of Fig. 1. This plot shows that in the SC state $\Gamma(T)$ continuously increases and reaches the MFL limit (i.e. $\Gamma \approx \omega_0$) for $T \approx T_c$.

With the extracted tanh-like form for $\Gamma(T)$ we now evaluate the temperature and frequency dependence of $\text{Im } \Sigma$ for parameters which also fit the real part (see below). In Fig.1 we compare our results with ARPES data on an optimally doped Bi2212 sample⁶ which support a scaling of $\text{Im } \Sigma$ as a function of ω/kT characteristic for a MFL. However, from the remarkable agreement of our fit with experiment as shown in Fig. 1 we conclude that the presence of a collective mode in the 48K data cannot be excluded. We will see below that this is also consistent with the observed temperature dependence of $\text{Re } \Sigma$ as required by the Kramers-Kronig transformation. It is worth noting that $\Gamma(T)$ was obtained from a fit to the quasiparticle weight at $(\pi, 0)$ whereas the experimental data shown in Fig. 1 are extracted from momentum distribution curves along the nodal direction. For large frequencies $\text{Im } \Sigma \rightarrow \lambda^2 N(0)$ and thus in our scaled representation Fig. 1 the saturation decreases with increasing temperature. Note that this saturation is due to the upper cutoff frequency of our bosonic spectrum at frequency $\omega_0 + \Gamma$.

Fig. 2a displays $\text{Re } \Sigma$ for parameters appropriate to

fit the data extracted from ARPES experiments on an optimally doped Bi2212 sample.²³ Note that parameters are the same for both temperatures except the broadening Γ which in the normal state is five times the value of that in the SC state. From our fit we thus again conclude that the increase of temperature alone is not sufficient in order to explain the change of $\text{Re } \Sigma$ from being significantly peaked at $T = 70\text{K}$ to the much broader structure at $T = 130\text{K}$. Instead the transition from $T < T_c$ to $T > T_c$ is accompanied by the transformation of the self-energy from mode-like to almost MFL behavior due to the broadening of the underlying bosonic spectrum Eq. (1).

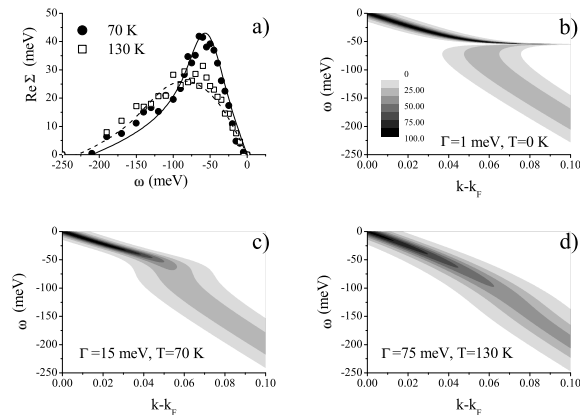


FIG. 2: a) $\text{Re } \Sigma(\omega)$ compared with experimental data from Ref. 23 for 70 K (solid line, circles) and 130 K (dashed line, squares). Parameters: $\omega_0 = 55\text{meV}$, $\omega_c = 400\text{meV}$, $\lambda^2 N(0) = 20\text{meV}$, $\Gamma(70\text{K}) = 15\text{meV}$, $\Gamma(130\text{K}) = 75\text{meV}$. (b-d) Contour plot of spectral functions for increasing values of Γ and temperature showing the gradual weakening of the kink feature.

In Figs. 2c-2d we show a contour plot of the spectral function $A_k(\omega) = 1/\pi \text{Im} 1/(\omega - \varepsilon_k - \Sigma(\omega))$ calculated for the two values of Γ as determined in Fig. 2a. The underlying bare dispersion is linearized around the Fermi momentum $\varepsilon_k \sim (k - k_F)$ since experimental data for $\text{Re } \Sigma$ in Fig. 2a have been obtained by subtracting the measured nodal dispersion from a noninteracting, linearized dispersion.²³

In addition Fig. 2b displays the spectral function for a rather narrow boson distribution ($\Gamma = 1\text{meV}$) at temperature $T=0\text{K}$. In this case the contour plot (Fig. 2b) reveals the occurrence of a break in the dispersion separating a strongly mass enhanced low energy part from a broad dispersive high energy feature. With increasing Γ (Figs. 2c, 2d) this break gradually changes into a kink which in the MFL limit ($\Gamma \gg \omega_0$) reduces to a slight change of slope in the dispersion.

As already discussed in the introduction the kink in the dispersion along the nodal direction is now well established in a large class of cuprates.⁷ Moreover ARPES

experiments on underdoped Bi2212 materials (cf. Fig. 2c of Ref. 7) clearly support the existence of a 'break' also in the nodal direction corresponding to the situation shown in Fig. 2b. Increasing doping or (and) increasing temperature leads to a decreased change of slope (i.e. less pronounced kink) around a characteristic binding energy (cf. Figs. 1b,e of Ref. 7). Comparing with the spectra shown in Fig. 2b-2d all these data suggest that the charge carriers are coupled to a bosonic spectrum which is rather sharply peaked well below T_c but gradually broadens with increasing temperature. In addition from the doping dependence of the kink we conclude that the minimum Γ is smaller in the underdoped regime.

III. BILAYER SPLITTING

Having analyzed the temperature and frequency behavior of the bosonic spectrum we now proceed by investigating its influence on the experimentally observed bilayer splitting in the SC and normal state of Bi2212 materials, respectively.

A. Formalism

Starting point is the following hamiltonian

$$H = \sum_{\mathbf{k}\sigma i} [\varepsilon_{\mathbf{k}} - \mu] c_{i,\sigma}^\dagger(\mathbf{k}) c_{i,\sigma}(\mathbf{k}) + \sum_{\mathbf{k}\sigma i \neq j} t_\perp(\mathbf{k}) c_{i,\sigma}^\dagger(\mathbf{k}) c_{j,\sigma}(\mathbf{k}) + \sum_{\mathbf{k}i} \Delta(\mathbf{k}) [c_{i,\uparrow}^\dagger(\mathbf{k}) c_{i,\downarrow}^\dagger(-\mathbf{k}) + c_{i,\downarrow}(-\mathbf{k}) c_{i,\uparrow}(\mathbf{k})] \quad (5)$$

where $i, j = 1, 2$ label the planes of the bilayer system. We restrict on an in-plane d-wave SC gap $\Delta(\mathbf{k}) = (\Delta_0/2)[\cos(k_x) - \cos(k_y)]$ and the interlayer hopping is parametrized as $t_\perp(\mathbf{k}) = (t_\perp^0/4)[\cos(k_x) - \cos(k_y)]^2$ in agreement with LDA²⁴ calculations and ARPES experiments.^{1,2} The bare energy spectrum ε_k in each plane is a tight-binding dispersion including up to fifth-neighbor hopping.²¹ A comparison of the corresponding Fermi surface (FS) with ARPES data from Ref. 1 is shown in the inset of Fig.3c for an interplane matrix element $t_\perp^0 = 40\text{meV}$. Diagonalization yields the four eigenvalues $\pm E_{1,2}(k) = \pm \sqrt{(\varepsilon_k - \mu \pm t_\perp(k))^2 + \Delta(k)^2}$.

The system Eq. (5) is now coupled to ICDW type fluctuations via the action

$$S = - \sum_q \int_0^\beta d\tau_1 \int_0^\beta d\tau_2 \sum_{i,j} \rho_q^i(\tau_1) \chi_q^{ij}(\tau_1 - \tau_2) \rho_{-q}^j(\tau_2) \quad (6)$$

where the susceptibility matrix contains both intra- ($\chi_q^\parallel \equiv \chi_q^{i=j}$) and interlayer ($\chi_q^\perp \equiv \chi_q^{i \neq j}$) contributions. Following the approach in Ref. 9 we consider an in-plane susceptibility which is factorized into an ω - and \mathbf{q} -dependent part, i.e. $\chi_q^\parallel(i\omega) = \lambda_\parallel^2 W(i\omega) J(\mathbf{q})$. Here, λ_\parallel denotes the intralayer coupling constant and $W(i\omega) =$

$-\int d\nu B(\nu)2\nu/(\omega^2 + \nu^2)$ is determined by the bosonic spectrum Eq. 1 for which we now consider a lorentzian shaped distribution function $F_{\omega_0, \Gamma}(\omega)$. $J(\mathbf{q})$ contains the charge-charge correlations which are enhanced at the four equivalent critical wave vectors $(\pm q_x^c, \pm q_y^c)$.

$$J(\mathbf{q}) = \frac{\mathcal{N}}{4} \sum_{\pm q_x^c; \pm q_y^c} \frac{\gamma}{\gamma^2 + 2 - \cos(q_x - q_x^c) - \cos(q_y - q_y^c)}. \quad (7)$$

\mathcal{N} is a suitable normalization factor introduced to keep the total scattering strength constant while varying γ . Note that for the chosen sign convention in Eq. (6) this kind of scattering leads to an effective attraction (in the static limit) between holes in the same plane. However, for the interlayer susceptibility the situation is different since the Coulomb repulsion perpendicular to the layers is only weakly screened and it is thus more likely to assume an effective repulsive interaction between holes in adjacent layers. For simplicity we therefore take in the following $\chi_q^\perp = -\chi_q^\parallel$ with $\lambda_\parallel = \lambda_\perp \equiv \lambda$ in order to describe the physical situation where charge enhanced regions in one layer correspond to charge depleted areas in the other layer. In this regard the situation is analogous to AF correlated spin fluctuations between the planes²⁵ when the spin-exchange potential couples exclusively even and odd electron states. We therefore consider our approach as complementary to models which are based on the magnetic resonance as the relevant collective mode. Preliminary investigations on charge-instabilities in a bilayer Hubbard-Holstein model²⁶ also give evidence for the presence of ICDW fluctuations in the odd channel.

The leading order one-loop contributions to the intra- ($\alpha = \parallel$) and interlayer ($\alpha = \perp$) self-energies read as

$$\underline{\underline{\Sigma}}^\alpha(k, i\omega) = -\frac{\lambda^2}{\beta} \sum_{q, ip} \chi_q^\alpha(ip) \underline{\underline{\tau}}_z \underline{\underline{G}}_0^\alpha(k - q, i\omega - ip) \underline{\underline{\tau}}_z \quad (8)$$

which in turn allows for the calculation of $\underline{\underline{G}}$ via

$$\underline{\underline{G}} = \underline{\underline{G}}_0 + \underline{\underline{G}}_0 \underline{\underline{\Sigma}} \underline{\underline{G}} \quad (9)$$

where the unperturbed Matsubara Greens function and self-energy are 4×4 matrices and are given by

$$\underline{\underline{G}}_0 = \begin{pmatrix} \underline{\underline{G}}_0^\parallel & \underline{\underline{G}}_0^\perp \\ \underline{\underline{G}}_0^\perp & \underline{\underline{G}}_0^\parallel \end{pmatrix}; \quad \underline{\underline{\Sigma}} = \begin{pmatrix} \underline{\underline{\Sigma}}^\parallel & \underline{\underline{\Sigma}}^\perp \\ \underline{\underline{\Sigma}}^\perp & \underline{\underline{\Sigma}}^\parallel \end{pmatrix}.$$

Finally by inverting the 4×4 matrix equation (9) the spectral function can be extracted from $A_k(\omega) = \text{Im}[G_{11}(k, \omega) + G_{33}(k, \omega)]$.

B. Results and Discussion

In Fig. 3 we present results for energy distribution curves (EDC) $I(k, \omega) = f(\omega)A(k, \omega)$ ($f(\omega)$ being the

Fermi function) in the normal (T=90K) and SC (T=10K) state and wave-vectors are indicated in the inset of Fig. 3c. Parameters (cf. caption to Fig. 3) were chosen in order to reproduce the ARPES line shape features in Ref. 1. Consider first the normal state spectra shown in Fig. 3a. Due to the large value of Γ in the underlying boson spectrum the bonding band (BB) gives rise to a broad high energy feature in the EDC at $\mathbf{k} = (\pi, 0)$. Together with the antibonding band (AB) quasiparticle peak the EDC thus displays a normal state peak-dip hump structure. The coupling to the flat boson spectrum naturally also affects the peak-hump separation at $\mathbf{k} = (\pi, 0)$ which therefore is slightly larger ($\approx 90\text{meV}$) than the bare bilayer splitting ($2t_\perp^0 = 80\text{meV}$). The MFL structure of both AB and BB spectral line shape is resolved in Fig. 3c. Upon scanning from $(\pi, 0)$ towards (π, π) first the AB peak goes through the chemical potential while the BB peak shifts to lower energy and sharpens due to the $\text{Im } \Sigma \sim \omega$ behavior. Finally between n8 and n9 also the BB peak crosses the Fermi energy. The AB and BB peak positions of the EDC curves from Fig. 3a are compared in Fig. 4 with ARPES data from Ref. 1.

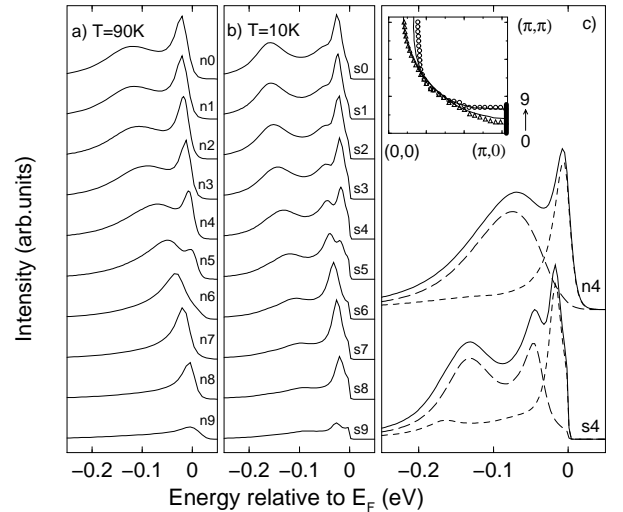


FIG. 3: ARPES spectra calculated for (a) normal state (T=90 K, $\Delta_0=0\text{meV}$, $\Gamma=100\text{meV}$), (b) SC state (T=10 K, $\Delta_0=20\text{meV}$, $\Gamma=10\text{meV}$). Spectra are taken along $(\pi, 0) \rightarrow (\pi, 0.24\pi)$, and labeled from 0 to 9 as shown in the inset of (c). The inset displays the calculated FS in comparison with data from Ref. 1. (c) shows selected spectra from (a) and (b), where dashed and dotted curves indicate BB and AB states respectively. Parameters: $\lambda=0.095\text{eV}$, $q_c = \pi/4$, $\omega_0=40\text{meV}$.

In the SC state the narrow bosonic distribution ($\Gamma = 10\text{meV}$) induces a strong mass enhancement for quasiparticles in the binding energy range up to the mean mode frequency ω_0 . Both AB and BB line shapes display the standard peak-dip hump structure where the hump is more pronounced for the BB (cf. curve s4 in Fig. 3c). The stronger renormalization of the BB band is due to the fact that (for our choice $\chi_q^\perp = -\chi_q^\parallel$) the self energies

of AB and BB bands

$$\underline{\underline{\Sigma}}^{A,B} = -\frac{\lambda^2}{2\beta} \sum \{(\chi_q^\parallel \pm \chi_q^\perp) \underline{\underline{\tau}}_z G_0^A \underline{\underline{\tau}}_z + (\chi_q^\parallel \mp \chi_q^\perp) \underline{\underline{\tau}}_z G_0^B \underline{\underline{\tau}}_z\} \quad (10)$$

are determined by fermionic excitations of BB and AB bands, respectively. Since the van-Hove singularity of the BB band is well separated from the chemical potential this results in a small AB self-energy and thus a relatively weak AB hump feature. In contrast the closeness of the AB van-Hove singularity to μ induces large BB self-energy effects and therefore a more pronounced BB hump structure.

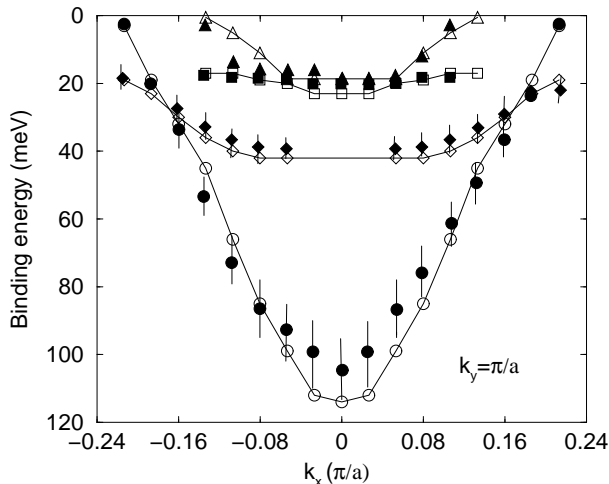


FIG. 4: Dispersion extracted from Fig.3 (open symbols); Filled symbols indicate experimental data from Ref. 1. Circles and triangles correspond to BB and AB normal state peaks, respectively; Diamonds and squares refer to BB and AB quasiparticle peaks in the SC state.

The SC low energy 'quasiparticle' peaks are confined to energies smaller than ω_0 and the corresponding quasiparticle weight decreases with increasing binding energy. As a consequence the quasiparticle peak of the bonding band is strongly suppressed at $\mathbf{k} = (\pi, 0)$ (curve s0 in Fig. 3b) and reemerges when the bare energy of the bonding band approaches ω_0 (curve s2 in Fig. 3b). In Fig. 4 where the low energy peak positions are shown as a function of k_x the dispersion of the BB therefore seems to be interrupted around $(\pi, 0)$ in agreement with the experimental data of Ref. 1. Moreover, Fig. 4 displays one of the main results of this paper. Whereas in the normal state the bilayer splitting is around 90meV the low energy peaks in the SC state are separated by $\approx 20\text{meV}$ only. As already discussed above the decreased bilayer splitting in the SC state is only due to the sharpening of the collective mode at low temperatures and not influ-

enced by any other parameter in our calculation.

IV. CONCLUSION

To conclude, we have shown that the self-energy as extracted from ARPES experiments can be consistently described within a model where the charge carriers are coupled to a bosonic distribution centered around some mean frequency ω_0 . The width Γ of this spectrum turns out to be strongly temperature dependent as can be concluded from the temperature dependent quasiparticle weight (cf. inset to Fig. 1), the evolution of the kink along the node (Figs. 2b-2d) and the corresponding change of $\text{Re } \Sigma$ in Fig. 2a with temperature. Within the ICDW scenario the associated scattering can account for the experimentally observed³ appearance of an additional peak-dip hump structure below T_c near the $(\pi, 0)$ points of the BZ (curve s4 in Fig. 3c). Moreover, the strong QP mass enhancement below T_c due to the small value of Γ leads to an apparent reduction of the bilayer splitting and a suppression of BB spectral weight around the $(\pi, 0)$ points (Fig. 4).

Note that phonons cannot account for the temperature dependence of the collective mode although their linewidth may undergo some sharpening upon entering the SC state. For temperatures well below the phonon frequency one can estimate the linewidth²⁸ from $\Gamma \approx \frac{\pi}{2} N(0) \lambda \omega_0^2$ which yields $\Gamma \ll \omega_0$ also for large coupling $\lambda \approx 1 \dots 2$. This is not enough to account for the strong damping as discussed above.

On the other hand the temperature dependent width of the bosonic spectrum can at least be made plausible within the ICDW scenario. At low temperatures the large intensity CDW mode at energy ω_0 and wave vectors $(\pm q_c, \pm q_c)$ is part of a band of excitations which for $q \rightarrow 0$ corresponds to the phason mode of the system. It is known²⁹ that the effective mass of the phason strongly increases with temperature due to the decreasing CDW gap inducing a significant broadening of the bandwidth of charge excitations. In fact, preliminary results obtained for the stripe phase of the Hubbard model²⁷ near the CDW transition have already revealed a rather continuous frequency spectrum in the charge susceptibility centered around q_c corresponding to the stripe periodicity. However, a more detailed investigation of this temperature dependence remains an interesting issue for future work.

V. ACKNOWLEDGMENTS

We would like to thank M. Grilli for helpful comments and a critical reading of the manuscript.

¹ D.L.Feng, N. P. Armitage, D. H. Lu, A. Damascelli, J. P. Hu, P. Bogdanov, A. Lanzara, F. Ronning, K. M. Shen,

H. Eisaki, C. Kim, J.-i. Shimoyama, K. Kishio, and Z.-X.

- Shen, Phys. Rev. Lett. **86**, 5550 (2001).
- ² Y.-D. Chuang, A. D. Gromko, A. Fedorov, Y. Aiura, K. Oka, Yoichi Ando, H. Eisaki, S. I. Uchida, and D. S. Dessau, Phys. Rev. Lett. **87**, 117002 (2001).
 - ³ A. D. Gromko, Y.-D. Chuang, A. V. Fedorov, Y. Aiura, Y. Yamaguchi, K. Oka, Yoichi Ando, D. S. Dessau, cond-mat/0205385.
 - ⁴ Y.-D. Chuang, A.D. Gromko, A.V. Fedorov, Y. Aiura, K. Oka, Yoichi Ando, D. S. Dessau, cond-mat/0107002.
 - ⁵ C. M. Varma, P. B. Littlewood, S. Schmitt-Rink, E. Abrahams, A. E. Ruckenstein, Phys. Rev. Lett. **63**, 1996 (1989).
 - ⁶ T. Valla, A.V. Fedorov, P. D. Johnson, B. O. Wells, S. L. Hulbert, Q. Li, G. D. Gu, N. Koshizuka, Science **285**, 2110 (1999).
 - ⁷ A. Lanzara, P. V. Bogdanov, X. J. Zhou, S. A. Kellar, D. L. Feng, E. D. Lu, T. Yoshida, H. Eisaki, A. Fujimori, K. Kishio, J. I. Shimoyama, T. Noda, S. Uchida, Z. Hussain, Z. X. Shen, Nature **412**, 510 (2001).
 - ⁸ J. C. Campuzano, H. Ding, M. R. Norman, H. M. Fretwell, M. Randeria, A. Kaminski, J. Mesot, T. Takeuchi, T. Sato, T. Yokoya, T. Takahashi, T. Mochiku, K. Kadowaki, P. Guptasarma, D. G. Hinks, Z. Konstantinovic, Z. Z. Li, and H. Raffy, Phys. Rev. Lett. **83**, 3709 (1999).
 - ⁹ G. Seibold and M. Grilli, Phys. Rev. B **63**, 224505 (2001).
 - ¹⁰ C. Castellani, C. Di Castro, M. Grilli, Phys. Rev. Lett. **75**, 4650 (1995).
 - ¹¹ G. Seibold and S. Varlamov, Proceedings of the *International Conference on Superconductivity, CMR & Related Materials*, Giens (2002); J. Supercond. **15**, 387 (2002).
 - ¹² H. Ding, J. R. Engelbrecht, Z. Wang, J. C. Campuzano, S.-C. Wang, H.-B. Yang, R. Rogan, T. Takahashi, K. Kadowaki, and D. G. Hinks, Phys. Rev. Lett. **87**, 227001 (2001).
 - ¹³ N. L. Saini and A. Bianconi (eds.), Proceedings of the *Third International Conference on Stripes and High T_c Superconductivity*; Int. J. Mod. Phys. **14**, (2000)
 - ¹⁴ J. E. Hoffman, E. W. Hudson, K. M. Lang, V. Madhavan, H. Eisaki, S. Uchida, J. C. Davis, Science **295**, 466 (2002).
 - ¹⁵ C. Howald, H. Eisaki, N. Kaneko, A. Kapitulnik, cond-mat/0201546.
 - ¹⁶ A. Kaminski, J. Mesot, H. Fretwell, J. C. Campuzano, M. R. Norman, M. Randeria, H. Ding, T. Sato, T. Takahashi, T. Mochiku, K. Kadowaki, and H. Hoehst, Phys. Rev. Lett. **84**, 1788 (2000).
 - ¹⁷ A. Kaminski, M. Randeria, J. C. Campuzano, M. R. Norman, H. Fretwell, J. Mesot, T. Sato, T. Takahashi, and K. Kadowaki, Phys. Rev. Lett. **86**, 1070 (2001).
 - ¹⁸ A. V. Puchkov, D. N. Basov, T. Timusk, J. Phys. Condens. Matter **8**, 10049 (1996).
 - ¹⁹ E. Abrahams and C. M. Varma, Proc. Natl. Acad. Sci. USA **97**, 5714 (2000).
 - ²⁰ Most of the ARPES data analyzed in the first part are for k-states along the diagonals where the SC gap vanishes anyhow.
 - ²¹ In order to reproduce the FS we choose $t_1 = -590$, $t_2 = 181$, $t_3 = -48.5$, $t_4 = -19.5$, $t_5 = 11$ (in meV).
 - ²² S. Engelsberg and J. R. Schrieffer, Phys. Rev. **131**, 993 (1963).
 - ²³ P. D. Johnson, T. Valla, A. V. Fedorov, Z. Yusof, B. O. Wells, Q. Li, A. R. Moodenbaugh, G. D. Gu, N. Koshizuka, C. Kendziora, Sha Jian, D. G. Hinks, Phys. Rev. Lett. **87**, 177007 (2001).
 - ²⁴ A. I. Liechtenstein, O. Gunnarsson, O. K. Andersen, R. M. Martin, Phys. Rev. B **54**, 12505 (1996).
 - ²⁵ A. I. Liechtenstein, I. I. Mazin, and O. K. Andersen, Phys. Rev. Lett. **74**, 2303 (1995).
 - ²⁶ G. Seibold, unpublished.
 - ²⁷ S. Varlamov and G. Seibold, Phys. Rev. B **65**, 075109 (2002).
 - ²⁸ P. B. Allen, Phys. Rev. B **6**, 2577 (1972).
 - ²⁹ G. Grüner, *Density Waves In Solids*, Addison-Wesley (1994).